Porcine skin visible lesion thresholds for near-infrared lasers including modeling at two pulse durations and spot sizes

C. P. Cain
Northrop Grumman
4241 Woodcock Drive
Suite B-100
San Antonio, Texas 78228-1330

G. D. Polhamus
W. P. Roach
U.S. Air Force
Air Force Research Laboratory
Human Effectiveness Directorate
Brooks City-Base, Texas 78235-5278

D. J. Stolarski
K. J. Schuster
K. L. Stockton
Northrop Grumman
4241 Woodcock Drive
Suite B-100
San Antonio, Texas 78228-1330

B. A. Rockwell
U.S. Air Force
Air Force Research Laboratory
Human Effectiveness Directorate
Brooks City-Base, Texas 78235-5278

Bo Chen
A. J. Welch
The University of Texas
Biomedical Engineering Department
Austin, Texas 78612

Abstract. With the advent of such systems as the airborne laser and advanced tactical laser, high-energy lasers that use 1315-nm wavelengths in the near-infrared band will soon present a new laser safety challenge to armed forces and civilian populations. Experiments in nonhuman primates using this wavelength have demonstrated a range of ocular injuries, including corneal, lenticular, and retinal lesions as a function of pulse duration. American National Standards Institute (ANSI) laser safety standards have traditionally been based on experimental data, and there is scant data for this wavelength. We are reporting minimum visible lesion (MVL) threshold measurements using a porcine skin model for two different pulse durations and spot sizes for this wavelength. We also compare our measurements to results from our model based on the heat transfer equation and rate process equation, together with actual temperature measurements on the skin surface using a high-speed infrared camera. Our MVL-ED_{50} thresholds for long pulses (350 μs) at 24-h postexposure are measured to be 99 and 83 Jcm^{-2} for spot sizes of 0.7 and 1.3 mm diam, respectively. Q-switched laser pulses of 50 ns have a lower threshold of 11 Jcm^{-2} for a 5-mm-diam top-hat laser pulse. [DOI: 10.1117/1.2338815]

Keywords: laser safety; laser injury; retina; cornea; visible lesion; model; infrared.

Paper SS04261RR received Dec. 30, 2004; revised manuscript received Oct. 11, 2005; accepted for publication Oct. 11, 2005; published online Sep. 5, 2006. This paper is a revision of a paper presented at the SPIE Conference on Laser Interaction with Tissue and Cells XV, Jan. 2004, San Jose, California. The paper presented there appears (unrefereed) in SPIE proceedings Vol. 5319.

1 Introduction

This study was initiated to provide relevant data, both experimental and modeling, for the effects of near-infrared laser pulses on the skin due to the growing application of high-energy lasers operating at wavelengths around 1315 nm. Near-infrared (NIR) lasers are becoming increasingly popular in various military, industrial, and medical applications. The development of high-power chemical oxygen iodine lasers (COIL) for use by the military has led to renewed interest in the safety of 1315-nm irradiation. Potential uses in new applications involve systems with nominal powers from the tens of kilowatts to the megawatt range. Though demonstrated to be one of the "safest" laser wavelengths with respect to human effects (requiring more energy than any other laser wavelength to cause injury), the types of injury associated with 1315 nm have been shown to be of particular concern.[1–3]

The American National Standards Institute (ANSI) standard Z136.1, 2000 (Ref. 4) defines wavelengths in the range of 1200 to 1400 nm to be NIR and recommends a constant maximum permissible exposure (MPE). MPE levels for skin exposure, which are established by the ANSI Z136.1 bioeffects subcommittee through threshold studies and modeling, are based on little experimental data in this wavelength regime. There has been some work researching the ocular effects of this wavelength region,[5,6] but little for skin effects. Unlike most other laser wavelengths, 1315-nm irradiation has been shown to cause damage at corneal, lenticular, and retinal sites. At relatively short exposure durations (i.e., 350 μsec) and large beam profiles at the cornea (5-mm diam), Zuclich et al.[3] found that threshold-level damage occurred at the back of the eye, involving the retina and the nerve fiber layers. On the other hand, Zuclich also found that for 1315- and 1318-nm laser beams smaller than 1 mm diam, threshold-level injury occurred at the cornea for exposure durations

Address all correspondence to Clarence Cain, Northrop Grumman, 4241 Woodcock Dr - Suite B-100, San Antonio, TX 78228; Tel: 210 536 1311; Fax: 210 534 0420; E-mail: clarence.cain@brooks.af.mil

1083-3668/2006/11(4)/041109/10/$22.00 © 2006 SPIE

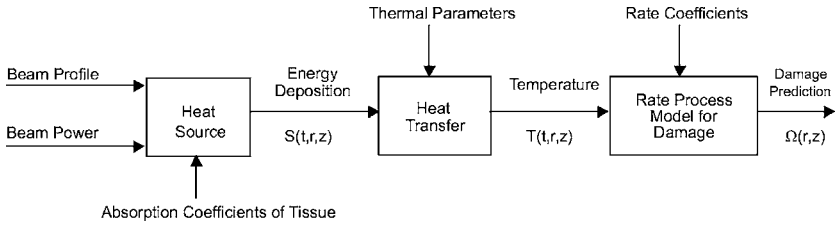

Fig. 1 Schematic of model for tissue injury from laser radiation.

from 350 μsec to 10 sec. This unusual threshold injury site dependence as a function of exposure duration and corneal beam size was presumed to be related to a probable change in optical properties of the cornea, such as thermal lensing, as a function of prolonged exposure and subsequent thermal injury, thus interfering with transmission of irradiation to the retina for the longer ($>$0.28 sec) exposures. Corneal threshold measurements have been reported by several researchers[7–9] for wavelengths between 1315 and 1356 nm for various spot size diameters and pulse durations. The reported thresholds range between 42 $\mathrm{Jcm^{-2}}$ at 300 μs to 1890 $\mathrm{Jcm^{-2}}$ for a 10-sec exposure of 1318 nm.

Several types of laser systems other than the COIL laser can produce wavelengths in the NIR region, with pulse durations ranging from Q-switched nanoseconds (ns) to continuous wave (cw). A commonly used laser that generates these wavelengths (1314 nm) is the neodymium:ytterbium lithium fluoride (Nd:YLF) laser. This specific system can develop energies from millijoules to joules, and can wavelength shift many nanometers by gain pulling. Another laser system, the Nd:YAG, can be operated at 1318 nm in the Q-switched mode to produce nanosecond pulses with many joules-per-pulse output. The data presented in this study are produced using a 1314-nm Nd:YLF laser system in the long-pulse mode (350 μs) with 3-J/pulse output and a Nd:YAG operating at 1318 nm in the short-pulse mode (50 ns) with a 5-J/pulse output.

Lasers operating at the 1320-nm wavelength have also become very popular and widely used in repairing artery anastomosis using human albumin solder (HAS). Several laboratories[10–12] have reported using the Nd:YAG laser operating at 1320-nm wavelength for laser-tissue welding of carotid arteries. These lasers heat up the solder used to weld the arteries together with minimal thermal damage. Lauto et al.[10] describe their welding of fresh canine arteries and report their results for various powers, energies, and temperature rises. For a 35-sec heating time, they reported energies used for soldering that ranged from 24 to 74 J and temperature increases of up to 25°C.

This study uses the Yucatan mini-pig (*Sus scrofa domestica*) as the model to determine the estimated dose for 50% probability of laser-induced damage (ED_{50}) to skin at wavelengths of 1314 nm (0.35 ms) and 1318 nm (50 ns) with single pulse exposures. The Yucatan mini-pig has higher anatomical similarity to human skin than the commonly used Yorkshire pig.[13] The Yucatan mini-pig skin is melanated and, on the flank, is of similar thickness to that on the human arm, which has high probability of accidental exposure. By using this model, the properties of human skin can be more closely approximated to gain a better understanding of the human laser-tissue interaction for the wavelength of interest. The data on porcine skin damage obtained from this study will contribute to the further understanding of laser injury mechanisms and will add to the existing data on laser skin effects, on which safety standards are based and which affect employment of these laser systems.

1.1 *Thermal Modeling*

The use of a mathematical model for predicting skin injury could be helpful in determining the key factors associated with these types of injury. Numerous models have been developed to predict laser energy absorption, source terms, temperature rise, and tissue damage. A schematic of such a combined model for ocular injury where light scattering is not significant is shown in Fig. 1.

In the early 1970's, Mainster, White, and Allen[14] solved the heat conduction equation of the form

$$\rho c\frac{\partial T}{\partial t} = Q + \frac{k}{r}\frac{\partial T}{\partial r} + \frac{\partial}{\partial r}\left(k\frac{\partial T}{\partial r}\right) + \frac{\partial}{\partial z}\left(k\frac{\partial T}{\partial z}\right), \qquad (1)$$

where cylindrical symmetry and thermally homogeneous media are assumed, and $T(r,z,t)$=temperature rise (K), t=time (s), k is conductivity ($\mathrm{W\cdot m^{-1}\cdot K^{-1}}$), c is specific heat ($\mathrm{J\cdot kg\cdot K}$), ρ is density ($\mathrm{kg\cdot m^{-3}}$), and $Q(r,z,t)$ is the source strength ($\mathrm{W\cdot m^{-3}}$).

The source strength for the tissue layers are, respectively,

$$Q_{PE} = hH_0\mu_{PE}\exp(-\mu_{PE}z) \quad (0 \le z \le d_{PE}), \qquad (2)$$

and

$$Q_{Ch} = hH_0\mu_{Ch}\exp(d_{Ch}\mu_{PE} - d_{PE}\mu_{PE} - \mu_{Ch}z)$$

$$(d_{PE} < z < d_{PE} + d_{Ch}), \qquad (3)$$

where $h(r)$=radial irradiance profile, H_0=the irradiance at $H(0,0,t)$, for $H(r,z,t)$=irradiance at the first and second layers, respectively, μ=absorption coefficient at the first and second layers ($\mathrm{m^{-1}}$), and d=thickness of the tissue layers ($\mathrm{m^{-1}}$).

Mainster, White, and Allen[14] used a finite difference solution to Eq. (1), and Vassiliadis, Christian, and Dedrick[15] developed a Green's function solution for symmetrical noncoherent sources. They also applied a rate process damage model to their temperature model. Welch, et al.[16] combined the rate process model with the finite difference model, and Takata et al.[17] expanded and modified the model to include multiple absorbing layers, reflection, blood perfusion, dam-

Table 1 Thermal properties of water.

Thermal properties of water		
Density(ρ)	1000	kg/m^3
Volumetric heat capacity (C)	4200	J/kgK
Thermal conductivity (k)	0.6	W/mK

Table 2 Coefficients of Arrhenius equation.

Coefficients of Arrhenius Equation		
Molecular collision frequency factor (A)	3.1E98	s^{-1}
Denaturation activation energy (E)	6.28E5	J/mole
Universal gas constant (R)	8.3143	J/mole/K

age, and steam formation. At the same time, Takata et al.[17] also developed a skin and corneal model of thermal injury. The damage model is based on the work of Henriques[18] in pig skin, and takes the form

$$\Omega(r,z) = A\int_0^t \exp(-E/RT)dt, \tag{4}$$

where A=molecular collision frequency factor (s^{-1}), E=deactivation energy (J/M), R=8.3143=universal gas constant (J/MK), $T=T(r,z,t)$=temperature (K), $\Omega(r,z)$=damage integral, and t=time at final recovery of temperature after exposure.

Henriques[18] used rate coefficients for Eq. (4) such that complete necrosis of the skin was associated with $\Omega=1$, and determined that $A=3.1\times10^{98}$ (s^{-1}) and $E=6.28\times10^5$(J/M).

Cain and Welch[19] tested the model temperature predictions for visible laser irradiation in the rabbit eye and determined it to be quite accurate for pulse durations exceeding approximately 10 msec. Welch[20] and Welch and van Gemert[21] have looked extensively at numerous factors affecting the model and its predictive power. Unfortunately, very little data on biological effects exist for the near-infrared wavelength of 1315 nm, and work is needed to evaluate the behavior of these models in this regime.

The skin model developed by Takata et al.[17] is similar in structure to the retinal model, though it uses skin geometries as well as optical and thermal properties of the skin. It also allows for appropriate alteration of the beam profile as the irradiation traverses the various layers of skin.

Takata et al.[17] pointed out the importance of the use of reliable parameters in the model, and particularly the selection of absorption coefficients for the ocular media or skin. The values for these critical parameters as used by Takata et al. were derived primarily from the work of Coogan, Hughes, and Mollsen,[22] Boettner,[23] and Geeraets et al.[24–26] One of the most challenging issues in the use of these models for the near-infrared region is the paucity of key parameters beyond 1200 nm (i.e., absorption coefficients and scattering).

1.2 *Models*

The laser-tissue interaction model used in this study consisted of three modules: 1. Monte-Carlo light propagation simulation; 2. finite element thermal model of heat conduction as indicated before; and 3. Henrique's rate process model of thermal damage. All modules used the same cylindrical grid system. Experimental values of the absorption coefficients (μ_a) and the reduced scattering coefficients (μ_s') were incorporated in a standard Monte-Carlo simulation for light scattering in two homogeneous regions of tissue (dermis and epidermis) with an air-tissue boundary condition. The simulation incorporated a Henyey-Greenstein (HG) phase function, an assumed anisotropic factor of $g=0.9$, and an index of refraction of tissue of 1.4. The resulting number of absorbed photons in a rectangular grid was scaled to define a source term Wcm^{-3} in an r, z array.

1.3 *Heat Conduction*

FEMLAB (COMSOL, Incorporated, Burlington, Massachusetts) code was used to compute the temperature increase during laser irradiation. At the end of the laser pulse, computed r, z temperatures were used as initial conditions to compute temperature relaxation regarding air-tissue convection ($h=500$ $Wm^{-2}K$). This value, which is ten times larger than the value reported by Takata et al.[17] for wet skin, compensates for water evaporation documented by Torres et al.[27] The thermal properties of water, specified in Table 1, were used in the FEMLAB simulation, since the tissue in this study is primarily composed of water. At each r, z point, the damage integral was computed as a function of time using the Arrhenius equation [Eq. (4)]. Values of A, E_0, and R for this computation are given in Table 2.

1.4 *Maximum Permissible Exposure from American National Standards Institute*

Safe laser exposures (MPE) to skin as specified by the ANSI standard[4] for this wavelength band are defined for various pulse durations and wavelengths. Since these limits are based on very little experimental data, there could be improvement to these limits as experimental data are obtained. Current standards are given in Table 3.

The parameter C_A equals a constant 5 for wavelengths between 1.050 and 1.4 μm with a 3.5-mm limiting aperture for all cases before.

From the ANSI standard, we find that the MPE for the wavelength of 1315-nm laser for pulse durations from 1 to 100 ns is 0.1 Jcm^{-2}, and then from 100 ns to 10 s, it is a function of the pulse duration. It varies from 0.1 Jcm^{-2} at

Table 3 MPE for skin exposure to a near-infrared laser beam for wavelengths between 0.400 and 1.400 μm.

Exposure duration (s)	MPE (J cm^{-2})	MPE (W cm^{-2})
10^{-9} to 10^{-7}	$2.0C_A\times10^{-2}$	
10^{-7} to 10	$1.1C_At^{0.25}$	
10 to $3\times10^{+4}$		$0.2C_A$

100 ns to 10 Jcm^{-2} for a 10-s pulse. We can compare these values with those reported in the literature for a variety of pulse durations. For 1315-nm lasers, we have measured threshold doses in our laboratory at two different spot sizes and for two different pulse durations (350 μs and 50 ns) on porcine skin (Yucatan mini-pig).

2 Methods

An array of laser exposures (with varying pulse energy) was placed on the flanks of Yucatan mini-pigs, and Probit analysis was used to determine the ED_{50}s for thermal injury. Two laser systems were employed to deliver either 1314-nm light at 0.35 ms or 1318-nm light at 50 ns. Laser exposures were accomplished with a laser system (Positive Light, Los Gatos, California) using a Nd:YLF rod, delivering 1314-nm light at 0.350-ms exposure time, and at various pulse energies. The laser produced a top-hat profile, and two experimental spot sizes (700 and 1300 μm) were used in this study. Spot sizes were measured using an Electrophysics IR camera (Electrophysics Corporation, Fairfield, New Jersy) with a Spiricon LBA 500 Laser Beam analyzer (Spiricon, Incorporated, Logan, Utah) and beam grabber card. The pulse duration is measured by an ET-3000 InGaAs (Electro-Optics Technology, Incorporated, Traverse City, Michigan) photodiode connected to a Tektronix TDS 220 oscilloscope (Tektronix, Incorporated, Beaverton, Oregon). Energy measurements are made with a Coherent-Molectron EPM2000 energy meter (Coherent Incorporated, Santa Clara, California) and JD25 and JD50 energy probes, which were placed after a 90/10 beamsplitter to collect 10% of the beam energy, and thus determine the actual energy delivered to the skin. An articulating arm laser beam delivery system from Laser Mechanisms, Incorporated (Farmington Hills, Michigan) was used to deliver the beam without having to move the subject. A metal "aiming ring" was attached to the end of the articulating arm, which maintained a constant distance between the arm's aperture and the subject. This allowed for precise positioning and distance control necessary to deliver exposures of known spot size, more accurate beam delivery, and a higher number of exposures per subject, resulting in a reduction of the total number of subjects required. The laser system setup is depicted in Fig. 2.

2.1 *Q-Switched Nanosecond Pulses*

A custom-built Q-switched Nd:YAG laser manufactured by Continuum Lasers was used to deliver 50-ns exposures to animal subjects. The laser was designed to yield high-power 50-ns pulses at 1318 nm. The maximum pulse energy of the laser was rated at 5 J, but in practice the output was limited to ~4 J per pulse because of the alignment required daily. A general schematic of the experimental setup is shown in Fig. 3. Two series of experiments were taken, one set for the smaller spot sizes (~2 mm diam) utilized the delivery arm as shown in Fig. 3, and the other set (5 mm diam) sent the beam directly to the animal skin.

2.2 *Animals*

Eleven female Yucatan mini-pigs (Lonestar Laboratory Swine, Seguin, Texas), weighing between 25 and 40 kg, were used in this study and all were between 3 and 8 months of age. Five separate flanks were used at each spot size with the 1314-nm laser, and three separate flanks were used for each spot size with the 1318-nm laser. The study fell under the animal use protocol titled "Evaluation of Laser Induced Corneal Lesions in the Dutch Belted Rabbit and Skin Lesions in the Yucatan Mini-Pig," which was approved by the Brooks City-Base, Texas Institutional Animal Care and Use Committee (IACUC). The animals involved in this study were procured, maintained, and used in accordance with the Federal Animal Welfare Act and the *Guide for the Care and Use of Laboratory Animals*, prepared by the Institute of Laboratory Animal Resources, National Research Council. Brooks City-Base, Texas has been fully accredited by the Association for Assessment and Accreditation of Laboratory Animal Care, International (AAALAC), since 1967.

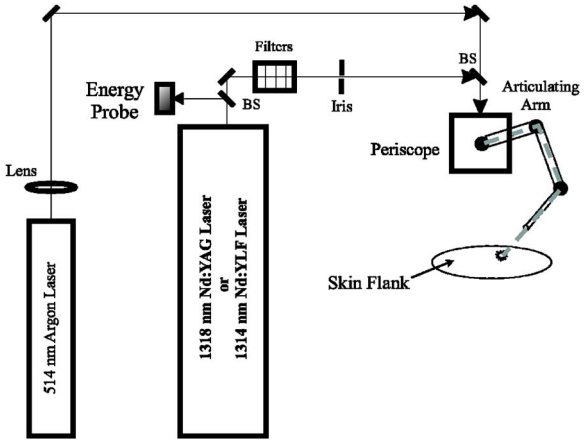

Fig. 3 Experimental setup for nanosecond experiment.

Only one of the animals was euthanized after exposure to obtain skin samples for the optical property measurements, and none after biopsy, since they were part of an animal-sharing program. Pigs were fed standard, commercially available diets, and had unlimited access to water. However, all solid food was withheld for 12 h prior to laser exposure and biopsy collection.

The pigs were sedated by single syringe injection of Tiletamine/Zolazepam (4 to 6 mg/kg) intramuscular (IM) and Xylazine (2.2 mg/kg) IM, and maintained on inhalation isoflurane anesthesia during all procedures. After sedation, hair on the flank was clipped using hand clippers, and the cleansed skin was inspected by each of three evaluators to check for redness, irritation, or other confounding marks. Physiological parameters were monitored throughout all procedures. Buprenorphine (0.05 to 0.1 mg/kg) was administered intramuscularly for analgesia after biopsies were complete. The animals were returned to their runs upon recovery to sternal recumbence from anesthesia.

For each subject, the flank to be exposed was marked with two 6×6-cm grids with a permanent-ink marker, making a total of 72 grid squares per flank. As previously mentioned, the distance between the articulating arm aperture and the skin was kept constant by the use of a metal device attached to the end of the arm. The animal, positioned on a table, did not have to be moved during procedures. Energy was delivered randomly to one grid at systematically varied intensities, and this process was then repeated on the second grid.

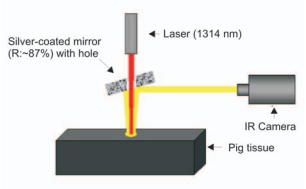

Fig. 2 Experimental setup for thermal dynamics imaging experiment.

Reading of skin exposure sites was performed acutely at one hour, and 24-h postexposure. Three trained lesion readers were used to evaluate the presence or absence of skin lesions. The readers used a lighted magnifying glass to examine the exposed skin area. The three readers independently examined the flank lesions immediately after all 72 exposures were accomplished. A lesion was recorded as a "yes" if at least two readers identified it as positive. One control biopsy was taken from flank skin located outside the exposure grids. The exposure grids were re-examined in the same way at 1- and 24-h postexposure, and two full-thickness biopsy specimens were taken at each time from sites that showed lesions. All biopsy skin samples were taken using a 6-mm skin biopsy punch, and immediately closed with a nonabsorbable suture, then topically medicated with Trio-mycin ointment. Harvested tissue was prepared for histopathologic analysis using 10% formalin solution, then blocked in paraffin and stained with hematoxylin/eosin (HE). An Olympus Vanox-S camera was used to magnify, evaluate and photograph the samples. Histological data will be reported at a later date.

Probit analysis[28] was the statistical method used to determine the estimated dose for 50% probability of laser-induced damage (ED_{50}) for the *in-vivo* skin model. Data points were entered into the Probit statistical analysis package and the ED_{50} was calculated along with fiducial limits at the 95% confidence level.

Measurements of laser-induced temperature increase in porcine skin samples were carried out using a high-speed IR focal plane array (FPA) camera sensitive in the mid-infrared (3 to 5 μm) spectral band (Phoenix model, Indigo Systems, Santa Barbara, California). To acquire reference IR image frames prior to laser exposure, the IR camera was operating in free-running mode at a frame rate of 100 Hz and image size of 256×256 pixels. The IR camera lens was extended to provide spatial resolution approximately 30 μm/pixel of 2-D temperature distribution at the laser spot on the skin surface.

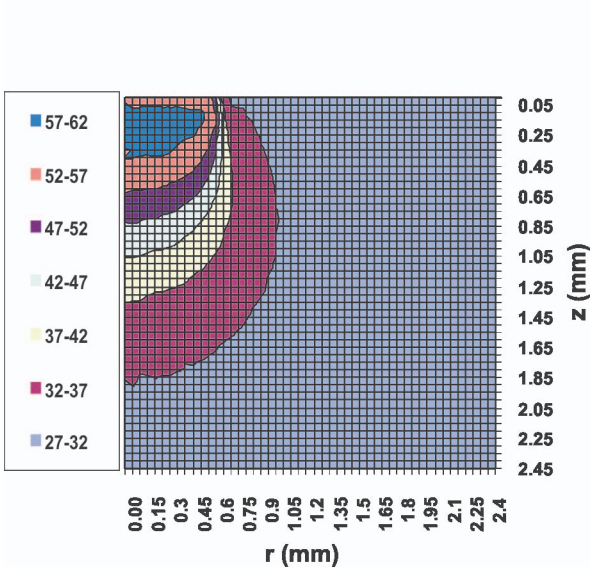

Fig. 5 Computed in-depth temperature distribution in both radial and axial directions at the end of laser pulse (350 μs): a pulse energy 1.1 J; wavelength 1314 nm; spot diameter 1.3 mm.

In our experiments, image acquisition was triggered 650 ms prior to laser exposure and a sequence of 500 frames was recorded to investigate laser-induced temperature increase. Because the IR image acquisition was not synchronized with pulsed laser exposure, there was uncertainty less than 10 ms in temporal position of the peak temperature recorded by the IR camera. However, due to relatively low thermal diffusivity of tissue, temperature change during the 10-ms time interval is negligible and can be ignored.

2.3 *Optical Properties*

In-vitro samples of pig skin were measured for estimates of optical properties (absorption coefficient μ_a and reduced scattering coefficient μ_s') as a function of wavelength (measured range 1000 to 1600 nm). Tissue samples were maintained at approximately 4 °C, and spectrophotometer measurements of reflection R and transmission T were made within 24 h of harvesting the skin samples for epidermis and dermis (see Table 4). Optical properties were obtained from R, T using the inverse adding-doubling technique.

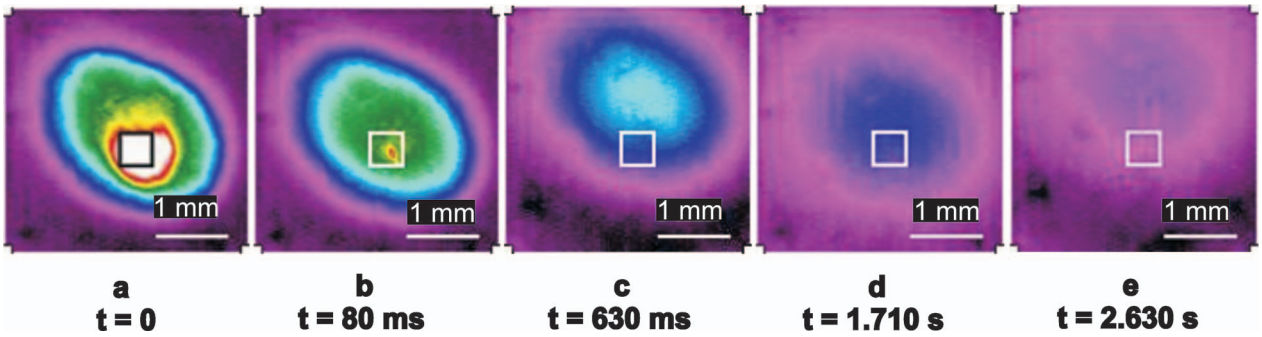

Fig. 7 Sequence of IR images with a 1.3-mm beam diameter (measured), and energy of 1.29 J.

Table 4 Optical properties of skin samples supplied by AFRL/HEDO and measured *in vitro* for Yucatan mini-pig epiderms and dermis.

Tissue (pigmented pig)	Wave (nm)	μa (1/cm)	μs (1/cm)	$\mu s'$ (1/cm)	g
epi_pig	1315	1.07	90.03	9.003	0.9
epi=epidermis,	1320	1.14	89.89	8.989	
der_pig	1315	1.19	89.77	8.977	0.9
der=dermis	1320	1.25	89.63	8.963	

μa(1/cm)=absorption coefficient. μs(1/cm)=scattering coefficient. $\mu s'$(1/cm)=reduced scattering.

3 Results

Visible lesion threshold measurements for two pulse durations with two spot sizes for each pulse duration are being reported, and enough data points were taken to provide the ED_{50}s and their fiducial limits at the 95% confidence level using Probit analysis. Results for the ED_{50}s using the long pulse (350 μs) are reported for both the 1- and 24-h postexposure readings in Table 5, along with their fiducial limits and slopes of the Probit curves (slope$=\delta p/\delta d$, where δp=delta probability and δd=delta dose). Fiducial limits as shown in the table for the 1.3-mm-diam spot size produces only $a\pm4\%$ spread around the ED_{50}, and this low value is due to the large number of data points recorded. Many of the laser exposures, especially for the smaller spot size, produced laser-induced breakdown (LIB) at the surface of the skin and we also heard a pop. However, no attempts were made to correlate the LIB with the damage thresholds. We do know that plasma shielding did affect the higher energy exposures, and that some very-high-energy pulses did not create lesions after 24 h that were observable at the 1-h reading.

Most lesions initially appeared as a blotched red coloring (erthema) near the center of the exposure site where the laser beam penetrated the skin. These red spots appeared almost immediately and many disappeared before the 1-h reading. Exposures sites were observed visually after 1 h, and most of the immediate lesions were no longer red splotches but very small discolorations in the skin. At the 24-h postexposure reading, more lesions could be clearly observed than were visible at 1-h postexposure for either spot size.

For the Q-switched 50-ns pulse exposures, attempts were made to utilize the smaller beam diameters at the skin, but this was not possible because of the LIB occurring in the air before reaching the skin. The irradiances in W/cm^2 for the nanosecond pulses were so large that the air broke down and shielded the skin from the laser pulses. Results for the two spot sizes used, 2 and 5 mm diameters, are listed in Table 6 for the same parameters at listed in Table 5. For the 5-mm spot size, fiducial limits calculated give a spread of only ±5% around the ED_{50} value. Most all of the visible lesion produced with the 2-mm-diam laser beam had LIB at the skin surface and a flash of light was visible. Since the mathematical models do not predict a spot-size dependency for pulse durations below one μsec, there should be no difference between the two spot sizes. Shielding by the plasma at the skin surface increased the minimum visible lesion (MVL) threshold by almost a factor of 4. The Q-switched pulses for the 5-mm-diam spots were not sent through the manipulating arm as all previous exposures to have enough energy at the skin for this large diameter of exposure. Even with the higher energy pulses, no LIB occurred nor was any flash visible. Profiles of the laser pulse at the skin surfaces were taken before and after each exposure session for all conditions, and these were used to measure the area of the exposure on the skin. Most of the pulses for the 2-mm-diam pulses produced LIB at the skin surface, and these are discussed later, but none of the 5-mm-diam exposures created plasma at the skin surface.

In Table 7, we compare the MPE values calculated from the ANSI standard to our MVL-ED_{50} threshold values measured for the larger spot sizes at the 24-h reading for both pulse durations. In the last column, we show the safety margin as the ratio of the ED_{50} to the MPE values, or how many times larger the ED_{50} is. We show that for both pulse durations it is 2 orders of magnitude larger than the MPE.

Measured temperature rises as a function of pulse energies are shown in Fig. 4 for the 1314-nm laser and with a spot size of 1.3-mm diameter (top-hat profile). Also shown are the Monte-Carlo FD model calculations for the temperature rise versus exposure energy at the center of the laser beam and just

Table 5 Visible lesion thresholds on Yucatan mini-pig skin at 1314 nm (for a 1.3-mm-diam, spot, *E* for 83 Jcm^{-2}=1.1 J, FD limits=+/−4%).

Skin exposures	MVL-ED_{50}	MVL-ED_{50}	Slope of Probit
1314 nm, 350-μs pulse	1-h reading	24-h reading	at 24 h
Yucatan mini-pigs	Fluence	Fluence	δprob/δdose
Flanks	Jcm^{-2}	Jcm^{-2}	
0.7 mm diam	111 (123 to 99)	99 (112 to 86)	3.3
5 pigs, 343 exposures			
1.3 mm diam	95 (101 to 89)	83 (85 to 81)	33
5pigs, 344 exposures			

Table 6 Visible lesion thresholds on Yucatan mini-pig skin at 1318 nm (for a spot of 5 mm diam *E* of 2.1 J for 10.5 Jcm^{-2}, FD limits=+/−5%).

Skin exposures	MVL-ED_{50}	MVL-ED_{50}	Slope of Probit
1318 nm, 50-ns pulse	1-h reading	24-h reading	at 24 h
Yucatan mini-pigs	Fluence	Fluence	δprob/δdose
Flanks	Jcm^{-2}	Jcm^{-2}	
2.0 mm diam	6.6 (8.0 to 5.3)	38.5 (51.3 to 30.6)	2.1
3 pigs, 216 exposures			
5.0 mm diam	6.5 (7.0 to 5.9)	10.5 (11.1 to 10.0)	10.7
3 pigs, 216 exposures			

below the skin surface. The distribution of temperature rises at the end of the laser pulse is shown in Fig. 5 for both radial and axial directions. For the parameters used in the model, this graph shows that the model temperatures that were calculated based on a laser pulse with a top-hat profile are moderately higher that those actually measured (Fig. 4). Also, there was a delay between the end of the laser pulse and the thermal imaging of up to 10 ms because the thermal camera was not synchronized with the laser pulse. Thus, hot spots in the laser profile and the uncertainty in the spot size contributed to the differences between the model and measurements.

The temperature-time decay on the surface of the skin was calculated for the 1.3-mm-diam spot, and these values compared to the actual temperature measurements as plotted in Fig. 6. This figure shows both the temperature measured with the infrared camera and calculated decay out to 4 sec for temperature rises above ambient, not actual temperatures as plotted in Fig. 4. The camera was free running at a hundred frames per second.

The model also calculated the damage integral output [Henriques' Eq. (4)] at each time step, giving values throughout the volume as a function of time. Assuming an Omega=1 as burn threshold, the model calculated that the maximum radius for burn was 1.6 mm and the axial depth of burn was calculated to be 2.1 mm for the parameters stated.

Values of μ_a and μ_s' for specific wavelengths used in our model calculations are given in Table 4. Our *in-vitro* optical property measurements from Yucatan mini-pig skin are consistent with published values for the visible spectrum. Our spectrophotometer measurements from 1.0 to 1.6 μm indicated that the reduced scattering coefficient is much larger than the absorption coefficient below a wavelength of 1.35 μm. Thus it is necessary to include the effects of light scattering at $\lambda=1.314$ μm in a Monte-Carlo simulation of light propagation to determine the heat source term for the heat conduction equation. We kept our samples in a water bath until measurements were made, and water absorption by the samples and evaporation in the spectrophotometer may have contaminated our measurements for wavelengths above 1.4 μm.

A sequence of the measured IR images is given in Fig. 7 for times out to almost 3 sec. Clearly there is a hot spot in the first frame at $T=0+$, and this could be due to either a hot spot in the laser beam profile, higher absorption properties on the skin, or both. The third and fifth frames are offset from the other frames, and we know that this is due to respiration artifacts, because the IR camera was fixed in space and the animal flank did move up and down with its breathing. A box is inserted to mark the selected area of maximum temperature.

Table 7 ANSI-MPE for skin compared to measured MVL- ED_{50}.

Yucatan mini-pigs	ANSI-MPE	MVL-ED_{50}	ED_{50}times
skin exposures	400 to 1400 nm	24-h reading	MPE
Wavelength/	Fluence	Fluence	Safety
pulse duration	Jcm^{-2}	Jcm^{-2}	margin
1314 nm, 350 μs	0.75	83 (85 to 81)	>100
1.3 mm diam			
1318 nm, 50 ns	0.1	10.5 (11.1 to 10.0)	100
5.0 mm diam			

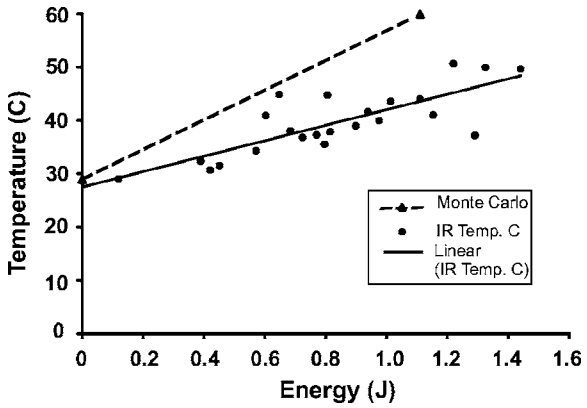

Fig. 4 Measured skin surface-temperature increases for varying pulse energies and Monte-Carlo FD model calculations using measured parameters.

At $t=0^+$ [Fig. 7(a)], the first frame after laser pulse occurs is shown. At $t=80$ ms [Fig. 7(b)], the hot spot begins to cool. At $t=630$ ms [Fig. 7(c)], respiration artifacts produce a noticeable upward shift of the temperature field with respect to the camera field of view. The hot spot is no longer visible, but the area temperature relaxation occurs from the radial center of the area. At $t=1710$ ms [Fig. 7(d)], the target area shifted back downward after breathing and continuing to cool. At $t=2630$ ms [Fig. 7(e)], the area is almost completely cooled, and the target shifts back upward due to breathing again.

4 Discussion

We have performed measurements on live pig skin and compare these thresholds with mathematical modeling to determine the thresholds for visible lesions, and then compare these trends with the ANSI safe exposure limits. Since the ANSI safe exposure limits for skin are based on both laser wavelength and exposure time, we have measured thresholds for two different pulse durations on two different laser spot sizes on the skin, as given in Tables 5 and 6. Only preliminary data have been reported[29] in the past, and that was for a spot size of only 0.25 mm in diameter due to laser pulse energy limitations. We had a higher energy laser and were therefore able to use much larger spot diameters of 0.7 and 1.3 mm. For the 0.7-mm spot, we measured an MVL-ED_{50} threshold of 111 Jcm^{-2} at the 1-h reading, and 99 Jcm^{-2} at the 24-h reading, which indicates that a few more lesions were observable after 24 h. It was observed but not recorded that during the higher energy exposures, a visible flash was seen and a loud pop was heard due to LIB occurring at the skin surface. This LIB could have had some affect on the thresholds and was not noticeable during the larger spot (1.3 mm) exposures. The occurrence of LIB is frequently seen for the large fluences in these exposures.[30] The MVL-ED_{50} thresholds for this larger spot size were somewhat lower (95 Jcm^{-2} at 1 h and 83 Jcm^{-2} at 24 h), and the differences could be due to a spot-size dependency, as predicted by the model for spot sizes smaller than about 1 mm in diameter. It could also have been due to the LIB at the surface for the smaller spot size. The slope of the Probit line was 33 for the 1.3-mm-diam spot, while only 3.3 for the 0.7-mm spot, which indicates more scatter in the data for the smaller spot. The ANSI exposure limit as given in Table 7 for this pulse duration (350 μs) is only 0.75 Jcm^{-2} or slightly more than two orders of magnitude below our 83 Jcm^{-2} for the ED_{50} measurement.

The skin surface-temperature measurements during and after the laser pulse for the 1.3-mm spot size is shown in Fig. 6 for pulse energies out to 1.4 J/pulse. For a comparison, the pulse energy at the ED_{50} value was 1.1 J, and this value indicates a temperature increase of 16°C rise over the 28°C skin surface ambient. The Monte-Carlo FD model predicted a 30°C rise due to the laser pulse using the parameters listed in Tables 1, 2, and 4.

MVL threshold measurements at the short pulse duration of 50 ns required special considerations to prevent LIB occurring in air, even before the laser pulse reached the pig skin. Pulse energies of 0.4 J/pulse when focused to spot sizes less than 1 mm diam produce an irradiance of more than 10^9 Wcm^{-2}. Because we were able to expose the skin with energies up to 3.2 J/pulse at 50 ns, we had to utilize spot diameters of at least 2 mm to prevent LIB in the air and shielding of the pulses for the skin exposures. Even for the 2-mm spot diameter, most of the recorded lesions indicated that the observers either saw a flash of light or heard a pop. At a spot diameter of 5 mm and with the 3.2 J/pulse maximum pulse energy available, the irradiances only reached a value of 3×10^8 Wcm^{-2} or well below the breakdown value for air or on the skin surface. The occurrence of LIB at the skin surface for thresholds lower than in free air is expected as free electrons are created at the skin surface by the large fluences from these exposures. The threshold for these phenomena is also reduced by significant linear absorption, up to a factor of 1000 reduction for very absorbing wavelengths in the far infrared.[30] We believe that LIB at the skin surface was the reason that the MVL-ED_{50} threshold for the 2-mm-diam spot (39 Jcm^{-2}, Table 6) was almost four times the value for the 5-mm-diam spot (10.5 Jcm^{-2}, Table 6). Also, no thermal model indicates that there will be a spot-size dependency of the thresholds for pulse durations of less that a microsecond. It is interesting to note that the MVL-ED_{50} thresholds at the 1-h reading were almost identical for both spot sizes.

Temperature calculation by the model for the 50-ns pulse had a computed temperature rise of a couple of degrees for no scattering and 8°C rise with scattering for the 5-mm, 2.2-J laser pulse. Thus we believe that the damage should be mechanical and not thermal. Certainly, we could have had LIB and acoustic shock waves without the indicators described before producing this visible skin damage.

5 Conclusions

We measure the minimum visible lesion thresholds in porcine skin for two different pulse durations and spot sizes and compare these values with a thermal damage model and the ANSI standards for the maximum permissible exposures at this wavelength. We use the standard finite element thermal model of heat conduction coupled with the Monte-Carlo light propagation simulation and feed the results into Henriques' rate process model of thermal damage. With this model, we can determine the maximum temperature reached during and after the laser pulse, temperature distribution throughout the tissue, and the damage levels reached within tissue. Absorption and

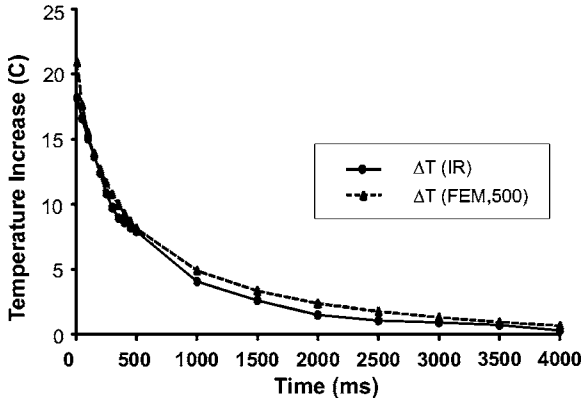

Fig. 6 Comparison between computed (upper-faced solid triangle) and measured (circle) time-dependent temperature relaxations (wavelength of 1314 nm, at the center of the beam, $h=500$ W/m^{2}K, $D=1.3$ mm).

scattering parameters were measured *in vitro* from freshly harvested skin from the same animal used for the high-speed temperature measurements, and these parameters were used in the model for all temperature calculations. The major difference between the parameters measured here and those measured many years ago during the first skin modeling attempts (Takata et al.[31]) is that in the past, light scattering within the skin was not understood well, and that internal scattered light was considered to be reflected back to the surface and be included in calculations by the reflection coefficient. The Takata model predicts the temperature rises adequately for large spot sizes but breaks down for very small spot sizes. We now know that light is scattered within the tissue and the light transport can be calculated using a scattering coefficient or reduced scattering coefficient[21] within the Monte-Carlo FE Model. Other researchers have reported porcine skin measurements that are similar to our measurements. The main difference between the our measurements and those reported by Du et al.[32] is that our measurements are from a porcine skin containing melanin granules and the theirs came from a domestic pig with white skin and no melanin.

We calculate the maximum permissible exposures from ANSI standards for this wavelength and these exposure times and find them to be two orders of magnitude lower than the ED_{50} thresholds measured. We cannot say for certain that there is a spot-size dependency for the long pulse durations (>1 μs) because of the very large field intensities for spot sizes below 1 mm and LIB occurring. However, we can now postulate that the MPE for skin at this wavelength of 1315 nm could be increased by an order of magnitude, i.e., from 0.75 Jcm^{-2} to 7.5 Jcm^{-2} at 0.35 ms, and for a pulse duration of 50 ns, it could be increased from 0.1 Jcm^{-2} to 1 Jcm^{-2} without jeopardizing the safety of exposures to the skin for this wavelength.

Acknowledgments

This research was supported in part by the Air Force AFOSR grant (2312A103), the Air Force Research Laboratory (contract F41624-97-D-9000 to Northrop Grumman IT), and a grant from Northrop Grumman IT to the University of Texas Biomedical Engineering Department, No. IRD2000STLAS02

References

1. B. E. Stuck, D. J. Lund, and E. S. Beatrice, "Ocular effects of laser radiation from 1.06 to 2.06 μm," *Letterman Army Institute of Research*, San Francisco, CA (1980).
2. J. A. Zuclich, H. Zwick, S. T. Schuschereba, B. E. Stuck, and F. E. Cheney, "Ophthalmoscopic and pathologic description of ocular damage induced by infrared laser radiation," *J. Laser Appl.* **10**, 114–120 (1998).
3. J. A. Zuclich, D. J. Lund, P. R. Edsall, B. E. Stuck, and G. T. Hengst, "High-power lasers in the 1.3 to 1.4 μm wavelength range: ocular effects and safety standards implications," *Proc. SPIE* **4246**, 78–88 (2001).
4. American National Standards Institute, "*American National Standard for the safe use of Lasers*," ANSI Standard Z136.1, New York (2000).
5. J. A. Zuclich, D. A. Gagliano, F. E. Cheney, B. E. Stuck, H. Zwick, P. R. Edsall, and D. J. Lund, "Ocular effects of penetrating IR laser wavelengths," *Proc. SPIE* **2391**, 112–125 (1995).
6. B. E. Stuck, D. J. Lund, and E. S. Beatrice, "Ocular effects of holmium (2.06 μm) and erbium (1.54 μm) laser radiation," *Health Phys.* **40**, 835–846 (1981).
7. B. E. Stuck, D. J. Lund, and E. S. Beatrice, "Ocular effects of laser radiation from 1.06 to 2.06 μm," *Letterman Army Institute of Research*, San Francisco, CA (1980).
8. D. J. Lund, B. E. Stuck, and E. S. Beatrice, "Biological research in support of project MILES," *Letterman Army Institute of Research Institute Report No. 96*, San Francisco, CA (1981).
9. W. P. Roach, B. Ketzenberger, M. B. Burton, and T. E. Johnson, "Corneal injury from 1318-nm single laser pulses," *Proc. SPIE* **4617**, 30–39 (2002).
10. A. Lauto, A. H. Hamawy, A. B. Phillips, P. B. Petratos, J. Raman, D. Felsen, W. Ko, and D. P. Poppas, "Carotid artery anastomosis with albumin solder and near infrared lasers: a comparative study," *Lasers Surg. Med.* **28**(1), 50–55 (2001).
11. J. M. Massicotte, R. B. Stewart, and D. P. Poppas, "Effects of endogenous absorption in human albumin solder for acute laser wound closure," *Lasers Surg. Med.* **23**(1), 18–24 (1998).
12. D. P. Poppas, R. B. Stewart, J. M. Massicotte, A. E. Wolga, R. T. Kung, A. B. Retik, and M. R. Freeman, "Temperature-controlled laser photocoagulation of soft tissue: in vivo evaluation using a tissue welding model," *Lasers Surg. Med.* **18**(4), 335–344 (1996).
13. T. A. Eggleston, W. P. Roach, M. A. Mitchell, K. Smith, D. Oler, and T. E. Johnson, "Comparison of two porcine (*Sus scrofa domestica*) skin models for in vivo near-infrared laser exposure," *Comparative Med.* **50**(4), 391–397 (2000).
14. M. A. Mainster, T. J. White, and R. G. Allen, "Spectral dependence of retinal damage produced by intense light sources," *J. Opt. Soc. Am.* **60**(6), 848 (1970).
15. A. Vassiliadis, H. C. Christian, and K. G. Dedrick, "Ocular laser threshold investigations," *USAF School of Aerospace Medicine*, Stanford Research Institute, Brooks Air Force Base, TX (1971).
16. A. J. Welch, C. P. Cain, and L. A. Priebe, "Model of thermal injury based on temperature rise in fundus exposed to laser radiation," *USAF School of Aerospace Medicine*, Brooks Air Force Base, TX (1975).
17. A. N. Takata, L. Goldfinch, J. K. Hinds, L. P. Kuan, N. Thomopoulis, and A. Weingart, Thermal Model of Laser-Induced Eye Damage, *Engineering Mechanics Division, IIT Research Institute*, Chicago, IL (1974).
18. F. F. Henriques, "Studies of thermal injury," *Arch. Pathol.* **43**, 489 (1947).
19. C. P. Cain and A. J. Welch, "Measured and predicted laser-induced temperature rises in the rabbit fundus," *Invest. Ophthalmol.* **13**(1), 60 (1974).
20. A. J. Welch, "The thermal response of laser Irradiated tissue," *IEEE J. Quantum Electron.* **QE-20**(12), 1471–1481 (1984).
21. A. J. Welch and M. J. C. Van Gemert, "Optical-thermal response of laser-irradiated tissue," *Lasers, Photonics, and Electro-Optics*, H. Kogelnik, Ed., Plenum Press, New York (1995).
22. P. S. Coogan, W. F. Hughes, and J. Mollsen, "Histologic and spectrophotometric comparisons of the human and Rhesus monkey retina and pigmented ocular fundus," *USAF School of Aerospace Medicine*, Brooks Air Force Base, TX (1974).
23. E. A. Boettner, "Spectral transmission of the eye," *Final Report on Contract AF 41(609)-2966 for the USAF School of Aerospace Medicine*, The University of Michigan, Brooks Air Force Base, TX (1967).

24. W. J. Geeraets, R. C. Williams, G. Chan, W. T. Ham Jr., D. Guerry III, and F. H. Schmidt, "The relative absorption of thermal energy in retina and choroid," *Invest. Ophthalmol.* **1**, 340 (1962).
25. W. J. Geeraets, R. C. Williams, G. Chan, W. T. Ham Jr., D. Guerry III, F. H. Schmidt, and W. J. Geeraets, R. C. Williams, M. Ghosh, W. T. Ham Jr., D. Guerry III, and R. Ruffin, "Light Reflectance from the ocular fundus: A means of estimating susceptibility to retinal burns," *Arch. Ophthalmol. (Chicago)* **69**, 612 (1963).
26. W. J. Geeraets and E. R. Berry, "Ocular spectral characteristics as related to hazards from lasers and other light sources," *Am. J. Ophthalmol.* **66**(1), 15–20 (1968).
27. J. H. Torres, M. Motamedi, J. A. Pearce, and A. J. Welch, "Experimental evaluation of mathematical models for predicting the thermal response of tissue to laser irradiation," *Appl. Opt.* **32**(4), 597–606 (1993).
28. D. J. Finney, *Probit Analysis*, 3rd ed., Cambridge University Press (1971).
29. T. E. Johnson, B. K. Ketzenberger, K. B. Pletcher, S. P. Wild, and W. P. Roach, "Skin exposures from 1318 nm laser pulses," *Proc. SPIE* **4257**, 355–362 (2001).
30. A. Vogel and V. Venugopalan, "Mechanisms of pulsed laser ablation of biological tissues," *Chem. Rev. (Washington, D.C.)* **103**, 577–644 (2003).
31. A. N. Takata, L. Zaneveld, and W. Richter, "Laser-induced thermal damage of skin," Report SAM-TR-77-38, Brooks Air Force Base, TX (Dec. 1977).
32. Y. Du, X. H. Hu, M. Cariveau, X. Ma, G. W. Kalmus, and J. Q. Lu, "Optical properties of porcine skin dermis between 900 nm and 1500 nm," *Phys. Med. Biol.* **46**, 167–181 (2001).